Electronic and Structural Variations of a Nickel(0) N-Heterocyclic Phosphenium Complex in Comparison to Group 10 Analogues

Leah K. Oliemuller, Curtis E. Moore, Christine M. Thomas*

Department of Chemistry and Biochemistry, The Ohio State University, 100 West 18th Avenue, Columbus, Ohio 43210, United States

Supporting Information Placeholder

ABSTRACT: The bonding interactions and electronic structure of a diphosphine pincer ligand featuring an N-heterocyclic phosphenium/phosphido (NHP^{+/-}) central moiety with nickel are explored. Treating Ni(COD)₂ with the diphosphine pincer ligand [PPP]Cl in the presence of a two-electron phosphine donor ligand PMe₃ generates chlorophosphine complex (PP^{CI}P)Ni(PMe₃) (**2a**). The cationic Ni complex [(PPP)Ni(PMe₃)][BPh₄] (**3a**) can be prepared by the subsequent halide abstraction from **2a** with NaBPh₄. The assignment of **3a** as a Ni⁰/NHP⁺ complex, based on analysis of structural parameters and computational investigations, lies in contrast to its previously reported group 10 M^{II}/NHP⁻ (M = Pd, Pt) analogues. The activation of O-H bonds across the Ni-P^{NHP} bond is demonstrated by the addition of isopropanol to afford the metal hydride species [(PP^{O/P}P)Ni(PMe₃)(H)][BPh₄] (**4**). Notably, the installation of a P-H bond in the NHP unit by treatment of **2a** with LiAlH₄ yields (PP^HP)Ni(PMe₃) (**6**). The ambiphilic nature of the P-H bond was demonstrated through reactivity studies of P-H bond cleavage in comparison to a Pd analogue (PP^HP)Pd(PPh₃) (**8**).

INTRODUCTION

In contrast to well-studied N-heterocyclic carbene ligands (NHCs), $^{1.2}$ reports of the isovalent group 15 analogues, N-heterocyclic phosphenium cations (NHP+s), have been far less prevalent in the literature. While NHCs are typically considered to be strong σ -donors and weak π -acceptors, NHP+s have demonstrated reciprocal electronic properties as weaker σ -donors and stronger π -acceptors, which may lead to different reactivity and binding properties in transition metal complexes. $^{3-}$ The strongly Lewis acidic character of these NHP+s in addition to the empty p-orbital on the phosphorus atom render the incorporation of these ligands into transition metal complexes as a promising strategy to facilitate the activation of σ -bonds across the metal-PNHP bond. $^{8-12}$

Unlike NHCs, NHP+s can adopt different geometries upon binding to a transition metal, associated with variations in metal-phosphorus bonding interactions (Chart 1).^{5,6} Transition metal NHP+ complexes typically feature a planar geometry about the central phosphorus atom. 13 This conformation is the result of σ-donation of the phosphenium's lone pair to the metal in combination with π -backbonding from a filled metal d orbital to the empty p orbital on the central phosphorus atom, leading to stronger, shorter metal-phosphorus bonds.^{5,6} A less common bonding scenario for the phosphenium can be envisioned in which the phosphorus-based lone pair remains nonbonding and the NHP⁺ ligand acts as a Z-type ligand, enforcing a pyramidal geometry upon metal coordination as a result of a donor-acceptor σ -bonding interaction from the metal to phosphorus.^{6,14,15} Notably, an alternative explanation for a pyramidal geometry about the central phosphorus atom is two-electron reduction of the NHP⁺ to form an N-heterocyclic phosphido (NHP⁻) ligand. In this scenario, metal-phosphorus bonding would be more covalent, the metal center would be formally oxidized by twoelectrons, and the pyramidal geometry would result from the remaining lone pair of electrons that is not participating in metal-ligand bonding. ^{6,16–18} Thus, NHP^{+/-} ligands can be considered as isolobal analogues of nitrosyl ligands, which are known to be redox active ligands through the two-electron interconversion of NO⁺ and NO^{-,19} However, unlike nitrosyl ligands, NHP^{+/-} ligands offer the added steric and electronic tunability of the heterocycle's carbon backbone as well as the substituents on the nitrogen atoms.

Chart 1. Different Binding Modes and Geometries of N-Heterocyclic Phosphenium/Phosphido Ligands.

$$\frac{\text{trigonal planar}}{\text{NHP*/M}^n}$$

$$\frac{\mathbb{R}}{\mathbb{R}} \oplus \mathbb{R}$$

$$\sigma\text{-donation only}$$

$$\frac{\sigma\text{-donation from M to P}}{\text{Trigonal pyramidal}}$$

$$\frac{\text{NHP*/M}^n}{\text{NHP*/M}^n}$$

Using an NHP-containing [PPP]⁺ framework,²⁰ our group has previously studied the NHP moiety's coordination to group 10 metals. In the case of Pd and Pt, the resulting dimeric species [(PPP)M]₂[PF₆]₂ (M = Pd (**A**), Pt (**B**)) feature bridging NHP⁺ phosphenium ligands and M^0 centers.¹⁶ The interconversion between the phosphenium and phosphido forms is highlighted in this system as the addition of PMe₃ to dimers **A** and

B cleanly generates the $[(PPP)M(PMe_3)][PF_6]$ (M = Pd (C), Pt (**D**)) monomers, whose assignments as M^{II}/NHP complexes are supported both experimentally and computationally (Chart 2).¹⁶ The ability to switch between NHP+/NHP- behavior was also demonstrated in the simultaneous electrophilic and nucleophilic behavior of the NHP moiety of [(PPP)Pt(PPh₃)][PF₆] (E) in the activation of E-H (E = O, S) bonds across the Pt-P^{NHP} bond to produce P-O/Pt-H and P-H/Pt-S products with opposite regioselectivity. 12 Consistent with the observed coordination behavior when using Pd or Pt, 16 coordination of the [PPP]Cl ligand to a Ni center was achieved by the oxidative addition of the P-Cl bond across the metal center to afford the Ni^{II}/NHP complex (PPP)NiCl (F) (Chart 2).21 However, careful stoichiometric control was required during the synthesis of F to avoid the formation of multimetallic species that, unlike the Pd and Pt analogues, cannot be cleaved into monomers via addition of exogenous phosphine donors. These synthetic difficulties previously prevented us from accessing monomeric Ni analogues of C-E for comparison or from exploring the activation of σ -bonds across the Ni-PNHP bonds.

Chart 2. Representative Dimeric and Monomeric Transition Metal NHP^{+/-} Complexes. ^{16,21}

Using the same PPP ligand scaffold, we sought to circumvent the formation of robust dimers by coordinating the [PPP]Cl ligand to a $\mathrm{Ni^0}$ center in the presence of additional phosphine donor ligands to stabilize monomeric species. Herein we describe these efforts as well as the reactivity of the resulting monomeric species toward bond activation processes using Ni as a cheaper alternative to other group 10 metals.

RESULTS AND DISCUSSION

Synthesis and Characterization of Cationic Nickel Complexes. In order to prevent the oxidative addition of the P-Cl bond across the Ni center, the chlorophosphine ligand precursor [PPP]Cl (1) was added to the Ni 0 starting material Ni(COD) $_2$ (COD = 1,5-cyclooctadiene) in the presence of an additional two-electron donor, trimethylphosphine (Scheme 1). The 31 P{ 1 H} NMR spectrum of the resulting product features a doublet of triplets at 144.0 ppm, a doublet of doublets at 23.7 ppm, and a doublet of triplets at -22.5 ppm. These three signals integrate in a 1:2:1 ratio and correspond to the halide-substituted NHP phosphorus center, two equivalent triarylphosphine sidearms, and the bound PMe $_3$ ligand, respectively. Single crystal X-ray diffraction confirmed the identity of the product as

four-coordinate tetrahedral Ni⁰ complex (PP^{Cl}P)Ni(PMe₃) (2a) (Figure 1).

Scheme 1. Synthesis of Four-Coordinate PPP-ligated Ni Complexes

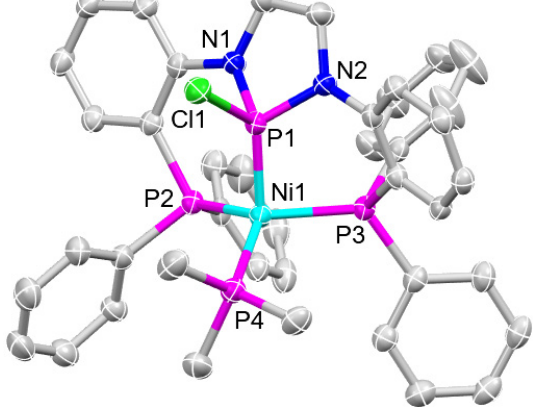


Figure 1. Displacement ellipsoid (50%) representation of **2a**. All hydrogen atoms have been omitted for clarity. Relevant bond distances (Å): Ni1-P1, 2.0299(7); Ni1-P2, 2.1454(6); Ni1-P3, 2.1640(6); Ni1-P4, 2.1682(7).

We attempted to synthesize a more sterically encumbered analogue of **2a** using the same procedure with a bulkier phosphine, triphenylphosphine. In contrast to **2a**, which can be cleanly isolated in the absence of excess PMe₃, the PPh₃ analogue (PP^{Cl}P)Ni(PPh)₃ (**2b**) more readily degrades into a mixture of previously reported complex **F** and dimers [(PPP)Ni]₂ and (PPP)₂Ni₃Cl₂ (Figure S4).²¹ Attempts to purify **2b** result in the observation of increasing amounts of PPh₃ by ³¹P {¹H} NMR spectroscopy, even when only one equivalent of PPh₃ is used in the initial reaction (Figure S5). We posit that the steric bulk of PPh₃ lends to its greater propensity to dissociate from transition metal complexes. In addition, the use of nonpolar solvents to remove free PPh₃ from the mixture results in further degradation, suggesting that the presence of some amount of free PPh₃ is needed to suppress this degradation (Figure S6).

Treatment of **2a** with NaBPh₄ at room temperature generates the halide-abstraction product [(PPP)Ni(PMe₃)][BPh₄] (**3a**) (Scheme 1). To synthesize a sterically encumbered analogue of **3a** using PPh₃, an alternative one-pot synthetic procedure was developed in an attempt to circumvent the aforementioned degradation of intermediate **2b** upon purification. This one-pot reaction resulted in the

formation of a single metal complex, [(PPP)Ni(PPh₃)][BPh₄] (**3b**). However, isolation of **3b** from remaining triphenylphosphine likewise resulted in similar product degradation to various unknown species, although to a much lesser extent than was observed for the neutral species **2b** (Figure S13). Cationic complex **3b** can, nonetheless, be isolated with a small amount (19%) of free PPh₃ present as the sole impurity. ³¹P {¹H} NMR spectra of **3a** and **3b** feature a significantly downfield-shifted P^{NHP} resonance (249.1 (**3a**), 248.7 (**3b**) ppm), indicative of the successful abstraction of the chloride on the central NHP phosphorus atom. ²² These chemical shifts are in agreement with those of the similarly downfield-shifted resonances of the central phosphorus atoms in the ³¹P {¹H} NMR spectra of the Pd and Pt analogues C (235.6 ppm), **D** (205.5 ppm), and **E** (198.8 ppm). ¹⁶

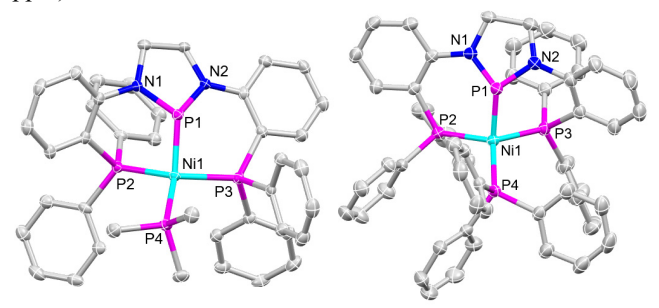


Figure 2. Displacement ellipsoid (50%) representations of the cationic portions of **3a** (left) and **3b** (right). All hydrogen atoms, BPh₄ counterions, and solvate molecules have been omitted for clarity. Relevant bond distances and angles are included in Table 1.

The solid-state structure of 3a shown in Figure 2 features a distorted pyramidal geometry about the central NHP phosphorus atom, where the sum of the angles around P^{NHP} is equal to 337.7° (Table 1). Notably, the previously reported group 10 analogues of 3a and 3b, C and D, which were described as MII/NHP complexes, adopt a more pyramidal geometry about the P^{NHP} atom, where the sum of the angles are 325.7° and 324.4°, respectively. 16 Furthermore, 3a features an angle of 141.7° between the N-P-N plane and the P^{NHP}-Ni bond vector, which is substantially more planar than the corresponding angles in \mathbf{C} and \mathbf{D} (130.9° in both). ¹⁶ In addition, the geometry of the Ni center in 3a is significantly more tetrahedral (τ_4 = 0.652),²³ while the metal centers in C ($\tau_4 = 0.328$) and D ($\tau_4 =$ 0.319) adopt distorted square planar geometries. 16 A greater shift toward the sterically preferred tetrahedral geometry at Ni is observed when using a bulkier phosphine in 3b ($\tau_4 = 0.803$) and the geometry about the P^{NHP} atom is also more planar (sum of angles = 341.6°, angle between N-P-N plane and Ni-PNHP bond vector = 145.1°) (Figure 2). However, the difference in geometry observed when varying the ancillary ligand is not nearly as large as the difference that results from varying the group 10 metal. The Ni-P^{NHP} distances in **3a** (2.0417(9) Å) and **3b** (2.0148(6) Å) are considerably shorter than the M-P^{NHP} distances in the Pd and Pt analogues (2.2535(6) and 2.2606(9) Å, respectively). 16 The short Ni-PNHP distances observed in 3a and 3b are comparable to the M-P distances reported in $[(PP)Ni(PMe_3)][BPh_4]$ **(G)** (1.9840(4))Å) $[(PP)Ni(PPh_3)][BPh_4]$ (H) $(2.0108(10)/2.0098(8) \text{ Å}),^{24}$ and $[(^{\text{Dipp}}NHP)Fe(CO)_3][PPh_4]$ (I; Dipp = 2,6-diisopropylphenyl) (1.989(1) Å) (Chart 3).²⁵ The latter complexes adopt a planar P^{NHP} geometry and were described as NHP⁺ phosphenium cations bound to M⁰ centers. (PPP)NiCl (F), which was described

as a Ni^{II}/NHP⁻ complex, has a longer Ni-P distance of 2.0903(6) Å.²¹ Even when accounting for the smaller covalent radius of nickel (1.20 Å in Ni vs 1.30 Å in Pd/Pt),²⁶ the M-P^{NHP} bonds in **3a** and **3b** are shorter than those of the Pd and Pt analogues, suggesting a stronger Ni-P^{NHP} bond. The distorted geometries of the Ni center toward tetrahedral, the less pyramidal P^{NHP} geometry, and the shorter Ni-P^{NHP} bond distances make the electronic assignment of **3a** and **3b** more ambiguous than their Pd and Pt analogues. Complexes **3a** and **3b** could either be described as Ni⁰/NHP⁺ complexes where the NHP ligand acts strictly as a Z-type ligand and the electron-rich Ni center donates into an empty orbital on P^{NHP}, or Ni^{II}/NHP⁻ complexes where the Ni-P^{NHP} bond is covalent and a lone pair is maintained on the central NHP phosphorus atom.

Chart 3. Representative Transition Metal NHP⁺ Complexes Reported by Thomas et al.²⁴ and Gudat et al.²⁵

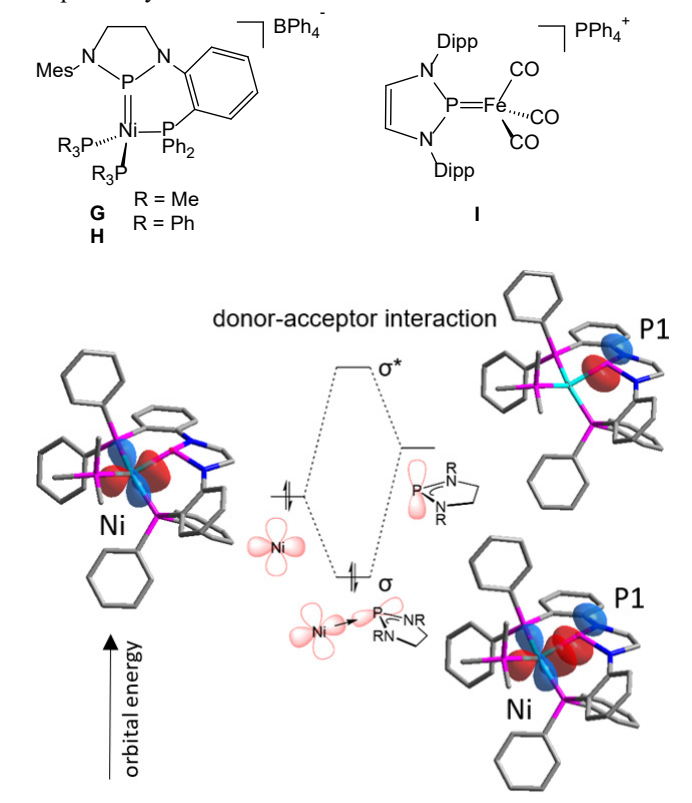


Figure 3. Pictorial representations of the calculated donor-acceptor interactions (NBO analysis) in 3a.

To provide further insight into the Ni-P^{NHP} bonding and electronic structure of the $[(PPP)Ni(PR_3)]^+$ cations in complexes $\bf 3a$ and $\bf 3b$, computational studies were performed using density functional theory (DFT) and natural bond orbital (NBO) analysis. Geometry optimizations were carried out starting from the crystallographically-derived Cartesian coordinates of the cationic portions of $\bf 3a$ and $\bf 3b$. The computed bond metrics agreed with those observed using X-ray crystallography (Table S5). The NBO analysis models the Ni-P^{NHP} interaction in $\bf 3a$ as a strong ($E_{\rm del} = 284.0$ kcal/mol) donor-acceptor interaction between a filled d orbital on Ni and an empty p orbital on P^{NHP} (Figure 3). A weaker ($E_{\rm del} = 260.6$ kcal/mol) Ni \rightarrow P^{NHP} donor-acceptor interaction is observed in $\bf 3b$, following the expected trend that the more electron-donating phosphine ligand in $\bf 3a$ gives rise to a more electron-rich Ni center and stronger Ni \rightarrow P interaction compared to $\bf 3b$. These results are consistent with a

Table 1. Selected Bond Distances (Å) and Angles (°) from Single Crystal X-ray Diffraction Data of Group 10 Cationic Complexes.

	$[(PPP)Ni(PMe_3)]^+$ $(3a)$	$ \frac{[(PPP)Pd(PMe_3)]^{+a}}{(C)} $	$ [(PPP)Pt(PMe_3)]^{+a} $ $ (\mathbf{D}) $	$[(PPP)Ni(PPh_3)]^+$ $(3b)$	$ \begin{array}{c} [(PPP)Pt(PPh_3)]^{+a} \\ (E) \end{array} $
M-P1 (Å)	2.0417(9)	2.2535(6)	2.2606(11)	2.0148(6)	2.2600(7)
M-P2 (Å)	2.1618(9)	2.3384(5)	2.3123(11)	2.1928(6)	2.3190(6)
M-P3 (Å)	2.1954(9)	2.3099(5)	2.3025(10)	2.1986(6)	2.3137(7)
M-P4 (Å)	2.2323(9)	2.4148(5)	2.367(1)	2.2391(6)	2.3787(6)
P2-M-P3 (°)	136.19(3)	161.993(19)	163.388(37)	122.35(2)	147.173(22)
P1-M-P4 (°)	131.58(3)	154.619(20)	154.962(33)	124.06(3)	149.085(22)
$ au_4{}^{ m b}$	0.652	0.328	0.319	0.803	0.455
$\Sigma_{ m P}{}^{ m c}$	337.7	325.7	324.4	341.6	319.2
NHP bend angled	141.7	130.9	130.9	145.1	126.2
16.1					

^aValues obtained from ref ¹⁶. ^bCalculation obtained using equation defined in ref ²³. $^{c}\Sigma_{P} = \text{sum of angles about P}^{NHP}$. ^dAngle between the metal-P^{NHP} bond vector and the N-P-N plane.

donor-acceptor interaction between a Ni⁰ center and a NHP⁺ fragment, where the NHP⁺ acts as a Z-type ligand to adopt a trigonal pyramidal geometry about the central phosphorus atom. An NBO analysis of Pt^{II}/NHP⁻ complex **D** revealed a covalent Pt-P^{NHP} NBO (41.6% Pt / 58.4% P),¹⁶ in stark contrast to Ni complexes **3a** and **3b**, which are better described as Ni⁰/NHP⁺ complexes.

Scheme 2. Reaction of ⁱPrOH with [(PPP)Ni(PMe₃)][BPh₄]

Cleavage of О-Н Bonds [(PPP)Ni(PMe₃)][BPh₄]. Since the bonding and electronic structure of 3a differs substantially from its Pt analogue, we next explored whether these differences in bonding manifested in divergent reactivity. E was reported to react with phenol upon heating for several days to generate [(PP^{OPh}P)Pt(H)(PPh₃)][PF₆] via oxidative addition of the O-H bond across the Pt-PNHP bond. 12 In contrast, the isoelectronic Co^I complex, (PPP)Co(PMe₃), was shown to activate PhOH in just 20 min at room temperature to afford (PPOPhP)Co(H)(PMe3),10 suggesting that metal-ligand cooperative bond cleavage may be more facile with first-row metals. The addition of PrOH across the $Ni-P^{NHP}$ bond indeed, in 3a, $[(PP^{O_iPr}P)Ni(H)(PMe_3)][BPh_4]$ (4) after 2 h at room temperature (Scheme 2). A new set of ³¹P{¹H} NMR resonances are observed for 4 at 124.1, 16.5, and -18.9 ppm, with the upfield shift in the PNHP signal suggesting successful RO addition to the previously unsubstituted central NHP phosphorus atom. A doublet of doublet of triplets at -13.0 ppm in the ¹H NMR spectrum of 4 is diagnostic for the formation of a nickel hydride (Figure S16). The large coupling constant (${}^2J_{H-PNHP} = 221 \text{ Hz}$) observed in both the ¹H NMR hydride signal and the ³¹P NMR spectrum indicates that the hydride ligand is oriented trans to the central P^{NHP} fragment, consistent with the large coupling constant (${}^2J_{H-}$ $_{PNHP}$ = 280 Hz) reported for the Pt analogue. ¹² Reaction of **3a** with phenol appears to afford a similar O-H oxidative addition product ([(PPOPhP)Ni(H)(PMe3)][BPh4]) due to the presence of a doublet of doublet of triplets in the metal hydride region of the ¹H NMR spectrum (${}^{2}J_{H-PNHP} = 225$ Hz) as well as similar resonances in the ³¹P and ³¹P{¹H} NMR spectra (Figures S22S23), but isolation and full characterization of this product was not pursued further based on evident similarities to 4.

The solid-state structure of 4 was determined using single crystal X-ray diffraction, confirming the trans relationship of the metal hydride and P^{NHP}, where the P^{NHP}-Ni-H angle is equal to 175.5(14)° (Figure 4). The Ni center in 4 adopts a distorted trigonal bipyramidal ($\tau_5 = 0.825$)²⁷ geometry. The Ni-P^{NHP} bond is elongated to 2.1123(6) Å compared to the Ni-P^{NHP} distance of 2.0417(9) Å in 3a as a result of an umpolung of the bonding interactions between Ni and P. The central PNHP atom in 4 now datively donates to the nickel center rather than the Ni→P donor-acceptor bonding interaction in 3a. An NBO analysis of the bonding in 4 after a DFT geometry optimization revealed that the Ni-P^{NHP} bonding interaction had a similar constitution to each of the other dative Ni-P interactions associated with the phosphine sidearms (Table S8). Conversely, the M-P^{NHP} bond distance in the Pt analogue changed very little (from 2.2600(7) Å to 2.2445(9) Å) upon O-H bond addition to \mathbf{E}^{12}

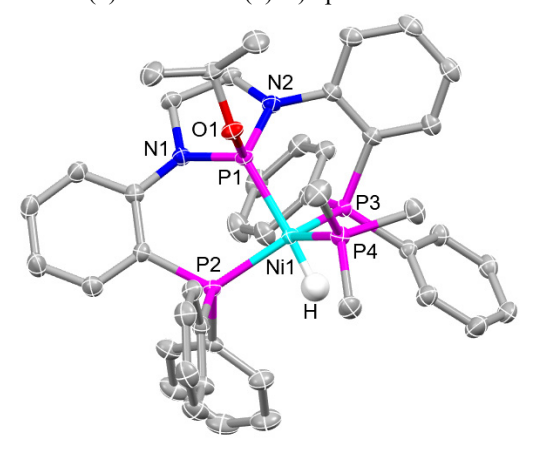


Figure 4. Displacement ellipsoid (50%) representation of the cationic portion of **4**. All hydrogen atoms not of interest, the BPh₄⁻ counterion, and solvate molecules have been omitted for clarity. Relevant bond distances (Å) and angles (°): Ni1-P1, 2.1123(6); Ni1-P2, 2.1541(6); Ni1-P3, 2.2056(6); Ni1-P4, 2.2257(6); Ni1-H, 1.31(3); P1-Ni1-H, 175.5(14).

Since isopropanol is often used as a source of hydrogen in catalytic transfer hydrogenation reactions, we further probed the reactivity of **3a** with PrOH in the presence of unsaturated substrates. Unfortunately, the addition of PrOH to **3a** in the presence of benzophenone at room temperature led to stoichiometric generation of **4**, with no transfer hydrogenation products formed.

Scheme 3. Thermal Decomposition of **3a** to (PP^{Ph}P)Ni(PMe₃) (5)

Attempts to drive catalytic transfer hydrogenation reactions at elevated temperatures were thwarted by the thermal instability of 3a. When solutions of 3a are heated to 80 °C for just one hour, the cationic complex decomposes to neutral complex (PPPhP)Ni(PMe₃) (5) via cleavage of a phenyl group from the BPh₄ counterion (Scheme 3). The structure of complex 5 was confirmed using single crystal X-ray diffraction, revealing that the geometry of the Ni center becomes more tetrahedral (τ_4 = 0.875) with the addition of a substituent on the central P^{NHP} atom (Figure 5). The upfield shift (89.3 ppm) of the central P^{NHP} atom resonance in the ³¹P{¹H} NMR spectrum of 5 spectroscopically supported the phenylation of the central PNHP atom (Figure S26) and BPh₃ was detected as a byproduct in the ¹H NMR spectrum of the crude reaction mixture (Figure S25). Phenyl transfer from the typically innocent counterion [BPh₄] has been observed upon coordination of the [PPP]+ ligand to a copper center.²⁸ In some cases, [BPh₄] has even been used as a phenylating agent.²⁹ An electrophilic phosphenium center susceptible to nucleophilic attack by the [BPh₄] counterion to generate 5 further supports the electronic assignment of 3a as a Ni⁰/NHP⁺ complex. In contrast, this reactivity is not observed in the PdII/NHP and PtII/NHP analogues, likely owing to their differing electronic structure.

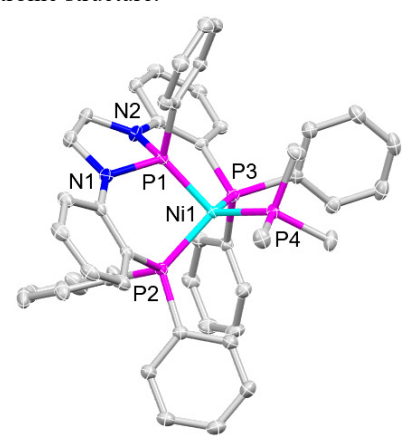


Figure 5. Displacement ellipsoid (50%) representation of **5**. All hydrogen atoms have been omitted for clarity. Relevant bond distances (Å): Ni1-P1, 2.0503(4); Ni1-P2, 2.1510(4); Ni1-P3, 2.1255(4); Ni1-P4, 2.1638(5).

Scheme 4. Installation of a P-H bond using LiAlH₄

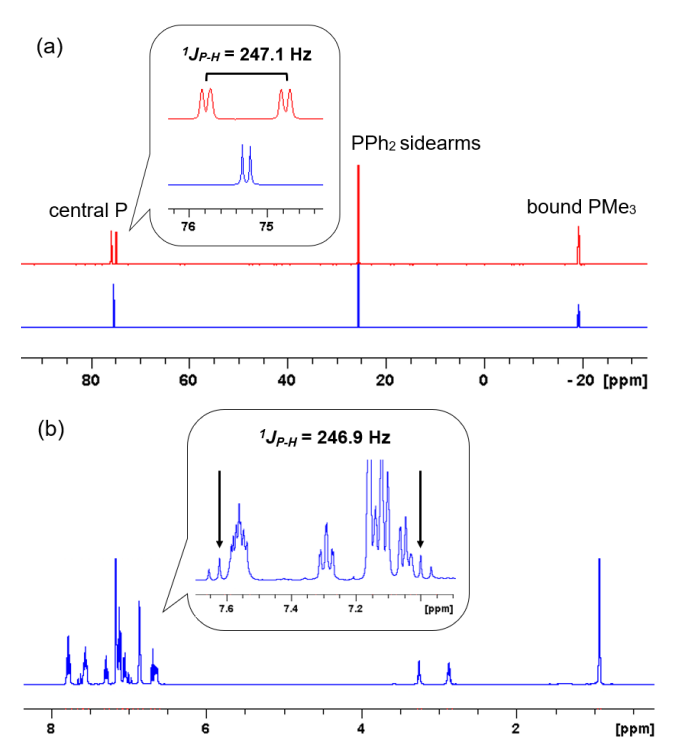


Figure 6. (a) A P-H bond is indicated by the additional coupling observed in the ³¹P NMR spectrum of **6** (top, red) compared to the ³¹P{¹H} NMR spectrum (bottom, blue). (b) A signal in the ¹H NMR spectrum of **6** with a similar ${}^{I}J_{P-H}$ coupling constant is centered around 7.31 ppm.

Synthesis, Characterization, and Reactivity of (PPHP)M(PMe3) Species. The dichotomy between NHP+ and NHP electronic descriptions allows for NHP units to engage in both nucleophilic and electrophilic reactivity. For example, Gudat et al. have demonstrated that the same NHP ligand in (NHP)Mn(CO)₄ and [(NHP)Fe(CO)₃] is susceptible to nucleophilic attack with H and methylation with methyl iodide, respectively. 9,25 In the opposite direction, we hypothesized that a PNHP-H bond may exhibit ambiphilic behavior such that it can be liberated as either a proton or a hydride with NHP or NHP leaving groups, respectively. The nickel system described herein is a promising candidate for exploring the ambiphilicity of the PNHP-H bond due to the assignment of the nickel complexes 3a and 3b as Ni⁰/NHP⁺ phosphenium complexes rather than Ni^{II}/NHP phosphido compounds. To demonstrate the proposed dual reactivity, a synthetic strategy to generate a P^{NHP}-H bond was developed. Addition of LiAlH₄ to 2a results in Cl⁻/H⁻ exchange to generate (PPHP)Ni(PMe₃) (6) (Scheme 4). Strong P-H coupling (${}^{1}J_{P-H}$ = 247.1 Hz) observed in the ${}^{31}P$ NMR spectrum of 6 confirms the successful formation of a P-H bond (Figure 6a). No upfield resonances typical of a metal hydride were observed in the ¹H NMR spectrum of **6**. However, a doublet of triplets is observed in the ¹H NMR spectrum overlapping with the aromatic resonances and centered at 7.31 ppm (Figure 6b). This signal has a ${}^{I}J_{P-H}$ coupling constant of 246.9 Hz, consistent with the coupling constant obtained from the ³¹P NMR data and providing further evidence of a PNHP-H bond in 6. A broad doublet centered at 7.31 ppm is clearly observed in the ²H NMR spectrum when LiAlD₄ is used as the hydride source to generate $(PP^DP)Ni(PMe_3)$ (6-d) (Figure S43). The ${}^{I}J_{P-H}$ coupling constant observed for 6 is considerably smaller than that observed for other transition metal NHP-H complexes, which typically range around 300-400 Hz. 10-12,30-33 Solution-phase IR

spectroscopy revealed a broad P-H stretch at 2083 cm⁻¹, which is a lower stretching frequency than the typical range reported for P^{NHP}-H bonds (2100-2200 cm⁻¹). For example, [(^{Dipp}NHP-H)Mn(CO)₄][PPh₄]⁻ features a v(P-H) stretching mode at 2120 cm⁻¹, and a stretch at 2161 cm⁻¹ is observed in the IR spectrum of (^{Dipp}NHP-H)Mn(H)(CO)₃.⁹ Thus, both the NMR and IR data indicate a weakened P^{NHP}-H bond in **6**.

The solid-state structure of **6** obtained using single crystal X-ray diffraction confirmed the installation of a P-H bond at the central P^{NHP} atom (Figure 7). The distance between the nickel center and the central P^{NHP} atom (2.0516(4) Å) remains similar to its chlorophosphine precursor **2a** (2.0299(7) Å). The P^{NHP}-H bond distance of 1.383(18) Å in **6** is consistent with other P^{NHP}-H transition metal complexes in the literature (1.3-1.4 Å).^{32,33} An elongated P^{NHP}-H bond in the solid state compared to previous compounds would be expected based on the solution state NMR and IR data; however, the inherent uncertainty in hydrogen positions determined via single crystal X-ray diffraction prevents rigorous comparisons between P-H distances.

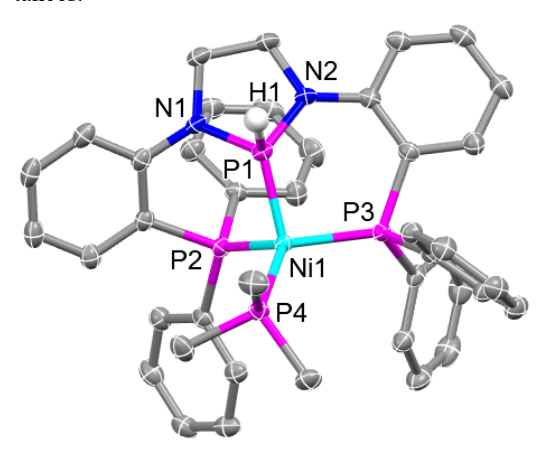


Figure 7. Displacement ellipsoid (50%) representation of **6**. Hydrogen atoms not of interest and solvate molecules have been omitted for clarity. Relevant interatomic distances (Å): Ni1-P1, 2.0516(4); Ni1-P2, 2.1502(4); Ni1-P3, 2.1283(4); Ni1-P4, 2.1583(4); P1-H1, 1.383(18).

In light of the weakened PNHP-H bond evidenced spectroscopically in 6, we anticipated that removal of the NHPbound hydrogen atom would be facile, allowing us to highlight the proposed ambiphilic nature of the P^{NHP}-H bond. Reactivity studies to assess the acidity or hydricity of the hydrogen atom in the P-H bond in 6 were performed. The additions of K[N(SiMe₃)₂] or Verkade's base (N(CH₂CH₂NMe)₃P) to 6 to deprotonate the P-H bond both resulted in no spectroscopically observed reaction. The addition of acids ([HNEt₃][BPh₄], 1.0 M HCl in Et₂O) in an attempt to protonate the P-H bond and release H2 gas also resulted in no spectroscopic change. Successful abstraction of a hydride from the P-H bond was, however, achieved using the Lewis acid B(C₆F₅)₃ to generate a cationic species (7) analogous to 3a with a $HB(C_6F_5)_3$ counterion (Scheme 5), as supported by identical ³¹P{¹H} NMR resonances (Figure S36). The $[HB(C_6F_5)_3]$ counterion was identified by ¹¹B and ¹⁹F NMR spectroscopy in agreement with chemical shifts reported in the literature (Figures S37-S38).34,35 The hydridic nature of the P-H bond in 6 lends credence to our description of **3a** and **3b** as NHP⁺/Ni⁰ phosphenium complexes.

Taking into consideration the notable differences in both the geometric and electronic structure between Ni⁰/NHP⁺ complexes 3a and 3b and their Pd and Pt M^{II}/NHP analogues C-E, we sought to synthesize a Pd analogue of 6 to probe the comparative electronic nature of the PNHP-H bond upon variation of the group 10 metal. In order to synthesize a palladium analogue of 6 using Pd(PPh₃)₄, a synthetic procedure for the generation of a [PPP]H ligand precursor was developed. The addition of one equivalent of KBEt₃H to [PPP]Cl produced the desired ligand [PPP]H (8) (Scheme 6). An upfield triplet for the central NHP phosphorus atom is observed in the ³¹P{¹H} NMR spectrum of 7 at 51.6 ppm and a signal with twice the integration is observed for the two equivalent triarylphosphine sidearms at -18.1 ppm. The P^{NHP} resonance in the ³¹P NMR spectrum features additional splitting (${}^{l}J_{P-H} = 235.9 \text{ Hz}$) into a doublet of triplets, confirming the successful formation of the P-H bond. The resonance for the P^{NHP}-H proton in the ¹H NMR spectrum is a doublet of triplets centered at 6.88 ppm and has a similarly large coupling constant (${}^{1}J_{H-P} = 235.0 \text{ Hz}$).

Scheme 5. Hydride abstraction of a P-H bond using a Lewis acid.

With ligand precursor **8** in hand, a Pd analogue of **6** was targeted. The reaction between **8** and Pd(PPh₃)₄ yields palladium complex **9** (Scheme 6), which exhibits spectroscopic features similar to those observed for **6**. The P^{NHP} resonance in the ³¹P NMR spectrum of **9** is located at 78.0 ppm and is a doublet of doublet of triplets where the ${}^{I}J_{P-H}$ coupling constant of 205.9 Hz is smaller than that of **6** (${}^{I}J_{P-H}$ = 247.1 Hz). In addition, solution-phase IR spectroscopy revealed a broad v(P-H) stretch at 2061 cm⁻¹ that is significantly lower in energy than that of **6** (v(P-H) = 2083 cm⁻¹). Although single crystals of **9** could not be grown, the spectroscopic data suggest that the Pd complex **9** is isostructural to Ni complex **6**, but with an even weaker P-H bond. We hypothesize that this weakened P-H bond is the result of a stronger M-P^{NHP} interaction owing to more covalent bonding in the case of Pd over its first-row counterpart Ni.

Scheme 6. Synthesis of a [PPP]H Ligand and Coordination to a Palladium Center

We then sought to determine if 9 would demonstrate different reactivity than the Ni analogue 6 to further support different electronic assignments. In contrast to 6, which had no reactivity with the strong base $K[N(SiMe_3)_2]$, Pd complex 9 was

susceptible to degradation upon deprotonation, as denoted by precipitation of dark insoluble solids from the reaction mixture (likely Pd(0)) and generation of a large quantity of PPh₃ (10.4:1 integration compared to remaining 9, Figure S56). In addition, 9 was treated with B(C₆F₅)₃ to examine its behavior toward Lewis acids. Treatment of 9 with one equivalent of B(C₆F₅)₃ produces a major product with features at 224.8, 14.0, and 12.5 ppm in its ³¹P{¹H} NMR spectrum, corresponding to a central P^{NHP} atom, two phosphine sidearms, and the bound PPh₃ ligand, respectively (Figure S57). Although a direct monomeric analogue of 3a has not been reported, the PMe₃ variant $\lceil (PPP)Pd(PMe_3) \rceil^+$ (E) features $P^{\hat{N}HP}$ and phosphine sidearm ³¹P{¹H} NMR resonances in similar positions at 235.6 ppm and 11.5 ppm. 16 Notably, we previously reported that the dimeric species [(PPP)Pd]₂²⁺ is formed upon addition of the cationic ligand [PPP] to Pd(PPh₃)₄. 16 This dimer was not identified spectroscopically as a byproduct of the reaction of 9 with B(C₆F₅)₃. suggesting that removal of a hydride from the central P^{NHP} atom after coordination to a Pd center may provide a unique avenue PPh₃-ligated previously elusive [(PPP)Pd(PPh₃)]⁺. Nonetheless, it appears that a hydride can be readily abstracted from the central phosphorus atom of both 6 and 9, but the increased reactivity of 9 with base in comparison to 6 is consistent with a more acidic P-H bond in 9, supporting a difference in the electronic structure and bonding of these two complexes.

CONCLUSION

In conclusion, the synthesis of monomeric Ni complexes featuring an NHP⁺ moiety has been developed using an exogenous phosphine ligand to prevent dimerization. (PP^{Cl}P)Ni(PMe₃) is treated with NaBPh₄, the halide is abstracted resulting in a cationic species [(PPP)Ni(PMe₃)][BPh₄] that is best described as a Ni⁰/NHP⁺ phosphenium complex, in contrast to analogous group 10 complexes reported as MII/NHP-(M = Pd, Pt) phosphido complexes. This differing assignment is supported structurally by a more planar central PNHP atom and a distorted tetrahedral nickel center as well as a computational investigation that revealed a Ni→P donor-acceptor interaction as the dominant bonding interaction. The O-H bond in PrOH can be activated across this Ni-P bond to readily afford a metal hydride complex [(PPOiPrP)Ni(PMe3)(H)][BPh4] via metal-ligand cooperativity. A P-H bond can be installed to the (PP^{Cl}P)Ni(PMe₃) precursor upon reaction with LiAlH₄ to produce (PP^HP)Ni(PMe₃). The phosphorus-bound hydrogen atom can subsequently be removed as H- using the Lewis acid $B(C_6F_5)_3$ to regenerate $[(PPP)Ni(PMe_3)]^+$, supporting the phosphenium character of the P^{NHP} atom in these Ni complexes. Although the P^{NHP}-H bond in the Ni species (PP^HP)Ni(PMe₃) could not be deprotonated using K[N(SiMe₃)₂], an analogous Pd complex (PPHP)Pd(PMe₃) was susceptible to degradation with the strong base K[N(SiMe₃)₂], highlighting the differing electronic description of the nickel system in comparison to its second and third row group 10 transition metal counterparts. Future studies will leverage the complex interactions between N-heterocyclic phosphenium/phosphido moieties and first-row transition metals toward the development of Earth-abundant transition metal catalysts.

EXPERIMENTAL SECTION

General Considerations. All manipulations were carried out under an inert atmosphere using a nitrogen-filled glovebox or standard Schlenk techniques. Glassware was oven-dried before use. All solvents

were degassed by sparging with ultra-high purity argon and dried via passage through columns of drying agents using a Seca solvent purification system from Pure Process Technologies. C₆D₆ and CD₂Cl₂ were purchased from Cambridge Isotopes Laboratories, dried over CaH₂, distilled, degassed by repeated freeze-pump-thaw cycles, and stored over pre-activated 3 Å molecular sieves. [PPP]Cl (1) was synthesized according to literature procedures.²⁰ NaBPh₄ (99.5%) was purchased from Acros Organics, and further dried under vacuum at 120 °C overnight prior to use. PPh3 was purchased from Alfa Aesar and dried under vacuum overnight prior to use. Isopropanol was purchased from Fisher Chemical, distilled, and stored over 3 Å molecular sieves. All other chemicals were purchased from commercial vendors and used without further purification. NMR data were recorded at ambient temperature unless otherwise stated on a Bruker DPX 400 MHz or Bruker AVANCE III HD 600 MHz instrument. Chemical shifts are reported in δ units in ppm referenced to residual solvent peaks (¹H and ¹³C{¹H}) NMR). $^{36\,31}P\{^1H\}$ and ^{31}P NMR chemical shifts are referenced using an 85% H₃PO₄ external standard (0 ppm). ¹¹B NMR chemical shifts are referenced using a BF₃•Et₂O external standard (0 ppm). ¹⁹F NMR chemical shifts are referenced using a CF₃COOH external standard (-76.55 ppm). Solution infrared spectra were recorded on a Bruker TEN-SOR II spectrometer controlled by OPUS software. Solid-state attenuated total reflection (ATR) infrared spectra were recorded on a Bruker ALPHA II spectrometer controlled by OPUS software. Microanalysis data (CHN) were collected by Midwest Microlab, Indianapolis, IN. High-resolution MS data were obtained using a Bruker Impact II instrument (Bruker Daltronics) with an electrospray ionization (ESI) source and quadrupole time-of-flight (Q-TOF) analyzer system.

(PP^{Cl}P)Ni(PMe₃) (2a). To a stirring solution of 1 (791 mg, 1.23 mmol) dissolved in THF (125 mL) was added PMe₃ (257 µL, 2.49 mmol) via micropipette. Ni(COD)2 (337 mg, 1.23 mmol) was dissolved in THF (20 mL) and added to the stirring solution of 1 and PMe₃. The solution was then concentrated in vacuo until orange solids precipitated. The solution was then filtered through Celite, and the remaining orange solid washed with hexanes (3 × 20 mL). Additional orange solid precipitated from the combined THF/hexanes filtrate. The resulting suspension was filtered through Celite again to collect the additional orange solid, which was washed with additional hexanes (3 \times 20 mL). The solids collected via both filtration steps were extracted with C₆H₆ (20 mL) and filtered through Celite. The benzene filtrate was dried in vacuo, yielding 2a as an orange solid (756 mg, 79%). Crystals of 2a suitable for X-ray diffraction were grown by storing a concentrated Et₂O solution of **2a** at -35 °C. ¹H NMR (400 MHz, C₆D₆): δ 7.79 (m, Ar-H, 4H), 7.37 (m, Ar-H, 4H), 7.28 (m, Ar-H, 2H), 7.11 (m, Ar-H, 2H), 7.05 (m, Ar-H, 4H), 7.02 (m, Ar-H, 2H), 6.88-6.81 (m, Ar-H, 8H), 6.75 (m, Ar-H, 2H), 3.87 (m, CH₂, 2H), 2.67 (m, CH₂, 2H), 0.99 (d, P(CH₃)₃, ${}^{2}J_{H-P} = 5.9$ Hz, 9H). ${}^{31}P\{{}^{1}H\}$ NMR (162.0 MHz, C₆D₆): δ 144.0 (dt, P^{NHP}, ${}^{2}J_{P-PPh2} = 72.4$ Hz, ${}^{2}J_{P-PMe3} = 10.7$ Hz, 1P), 23.7 (dd, PPh₂, ${}^{2}J_{P-PNHP} = 72.1$ Hz, ${}^{2}J_{P-PMe3} = 15.6$ Hz, 2P), -22.4 (dt, PMe₃, ${}^{2}J_{P-PMe3} = 15.6$ Hz, 2P), -22.5 (dt, PMe₃, ${}^{2}J_{P-PMe3} = 15.6$ Hz, -22.5 (dt, PMe₃, ${}^{2}J_{P-PMe3} = 15.6$ Hz, -22.5 (dt, PMe₃, ${}^{2}J_{P-PMe3} = 15.6$ Hz, -23.5 (dt, PMe₃, ${}^{2}J_{P-PMe3} = 15.6$ $PPh2 = 15.7 \text{ Hz}, ^2J_{P-PNHP} = 11.1 \text{ Hz}, 1P). ^{13}C\{^1H\} \text{ NMR } (150.9 \text{ MHz}, 1P). ^{13}C\{^1H\}$ C_6D_6): δ 147.5 (m, ipso), 141.1 (m, ipso), 140.5 (m, ipso), 134.6 (s), 133.8 (m), 133.0 (m), 130.4 (s), 128.7 (m, *ipso*), 128.6 (s), 128.5 (s), 128.4 (s), 127.7 (m), 122.2 (s), 120.6 (s), 45.6 (d, CH₂CH₂, ${}^{2}J_{C-PNHP}$ = 5.5 Hz), 20.1 (m, P(CH₃)₃). Anal. Calcd for C₄₁H₄₁NiN₂P₄Cl: C, 63.15; H, 5.30; N, 3.59. Found: C, 63.14; H, 5.70; N, 3.24.

[(PPP)Ni(PMe₃)][BPh₄] (3a). To a stirring solution of 2a (311 mg, 0.399 mmol) dissolved in THF (250 mL) was added a solution of NaBPh₄ (136 mg, 0.397 mmol) dissolved in THF (20 mL). The solution immediately turned dark purple-pink and was stirred at room temperature for 2 h. The solvent was then removed from the reaction mixture in vacuo. The crude dark purple-pink solid was suspended in C₆H₆ (250 mL) and filtered through Celite, collecting purple solids and removing a dark red filtrate. The remaining purple solid was extracted with CH₂Cl₂ (40 mL) and filtered through Celite. The solvent was removed from the CH₂Cl₂ filtrate in vacuo, yielding 3a as a purple residue (251 mg, 59%). Crystals of 3a suitable for X-ray diffraction were grown via slow evaporation of a dilute solution of 3a in C₆H₆. ¹H NMR (600 MHz, CD₂Cl₂): δ 7.53-7.41 (m overlapping signals, Ar-H, 12H), 7.36-7.31 (m overlapping signals of BPh₄, 8H, and Ar-H, 4H), 7.24-7.17 (m overlapping signals, Ar-H, 10H), 7.07 (m, Ar-H, 2H), 7.01 (m, BPh4, 8H), 6.86 (m, BPh₄-, 4H), 3.61 (m, CH₂CH₂, 2H), 2.47 (m, CH₂CH₂, 2H), 0.97 (d, P(CH₃)₃, ${}^2{J_{H-P}}$ = 7.0 Hz, 9H). 31 P{ 1 H} NMR (242.9 MHz, CD₂Cl₂): δ 249.1 (dt, P^{NHP}, ${}^2{J_{P-PPh_2}}$ = 32.3 Hz, ${}^2{J_{P-PMe_3}}$ = 46.3 Hz, 1P), 19.2 (d, PPh₂, ${}^2{J_{P-NHP}}$ = 32.2 Hz, 2P), -27.1 (d, PMe₃, ${}^2{J_{P-NHP}}$ = 46.6 Hz, 1P). 13 C{ 1 H} NMR (150.9 MHz, CD₂Cl₂): δ 164.5 (m, BPh₄, *ipso*), 145.5 (m, *ipso*), 136.6 (m, *ipso*), 136.3 (s, BPh₄), 134.7 (s), 134.5 (m, *ipso*), 133.3 (m), 132.6 (s), 132.5 (m), 130.9 (m), 129.3 (m), 128.7 (s), 127.6 (s), 126.0 (m, BPh₄), 125.5 (m), 122.9 (m, *ipso*), 122.7 (s), 122.1 (s, BPh₄'), 48.7 (s, CH₂CH₂), 18.5 (br d, P(CH₃)₃, ${}^2{J_{C-PNHP}}$ = 23.2 Hz). 11 B NMR (192.5 MHz, CD₂Cl₂): δ -6.9. Anal. Calcd for C₆₅H₆₁NiBN₂P₄: C, 73.40; H, 5.78; N, 2.63. Found: C, 74.07; H, 5.92; N, 3.91.

[(PPP)Ni(PPh₃)][BPh₄] (3b). To a stirring solution of 1 (106 mg, 0.165 mmol) and PPh₃ (43 mg, 0.16 mmol) dissolved in THF (8 mL) was added a solution of NaBPh₄ (56 mg, 0.17 mmol) dissolved in THF (2 mL). Ni(COD)₂ (45 mg, 0.16 mmol) was dissolved in THF (10 mL) and added to the stirring reaction mixture. The cloudy yellow solution immediately turned dark purple-pink and was stirred at room temperature for 2 h. The solvent was then removed from the reaction mixture in vacuo. The resulting oily solid was washed with C₆H₆ (6 mL), then extracted with CH2Cl2 (4 mL) and filtered through Celite. The solvent was removed from the filtrate in vacuo yielding 3b as a purple-pink solid (161 mg, 78%). Crystals of 3b suitable for X-ray diffraction were grown via vapor diffusion of n-pentane into a concentrated THF solution of **3b** at -35 °C. ¹H NMR (600 MHz, CD₂Cl₂): δ 7.57 (m, Ar-H, 2H), 7.36-7.33 (m overlapping signals of BPh₄, 8H, and Ar-H, 4H), 7.30 (m, Ar-H, 4H), 7.27-7.25 (m, Ar-H, 2H), 7.24-7.22 (m, Ar-H, 2H), 7.21-7.18 (m, Ar-H, 4H), 7.10-7.06 (m overlapping signals of PPh₃, 6H, and Ar-H, 4H), 7.04-7.01 (m overlapping signals of BPh₄, 8H, and Ar-H, 2H), 6.97-6.91 (m overlapping signals of PPh₃, 6H, and Ar-H, 2H), 6.87 (m overlapping signals of BPh₄, 4H, and Ar-H, 2H), 6.47 (m, PPh₃, 3H), 3.66 (m, CH₂CH₂, 2H), 2.50 (m, CH₂CH₂, 2H). ³¹P{¹H} NMR (242.9 MHz, CD₂Cl₂): δ 248.7 (br dt, P^{NHP}, ${}^{2}J_{P-PPh2} = 29.7$ Hz, $^{2}J_{P-PPh3} = 35.9 \text{ Hz}, 1P$), 29.7 (br dt, PPh₃, $^{2}J_{P-PPh2} = 9.1 \text{ Hz}, ^{2}J_{P-PNHP} =$ 35.9 Hz, 1P), 16.6 (br dd, PPh₂, ${}^{2}J_{P-PPh3} = 9.1$ Hz, ${}^{2}J_{P-NHP} = 28.8$ Hz, 2P). ¹³C{¹H} NMR (150.9 MHz, CD₂Cl₂): δ 164.5 (q, BPh₄, ipso), 146.1 (br s, ipso), 144.5 (m, ipso), 136.3 (s, BPh₄-), 135.1 (m, ipso), 134.6 (s), 134.4 (m, *ipso*), 134.1 (s), 134.0 (m), 133.4 (m), 133.1 (br s, ipso), 132.8 (m), 130.9 (s), 130.2 (s), 129.8 (s), 129.1 (s), 128.9 (m), 128.7 (s), 126.0 (s, BPh₄), 125.7 (s), 123.9 (s), 122.2 (s, BPh₄), 49.9 (br s, CH₂CH₂). ¹¹B NMR (192.5 MHz, CD₂Cl₂): δ -6.8. Anal. Calcd for C₈₀H₆₇NiBN₂P₄: C, 76.88; H, 5.40; N, 2.24. Found: C, 75.14; H, 6.14; N, 2.38. Complex 3b is extremely air and moisture sensitive when removed from an inert atmosphere. The low C value can be explained through the partial oxidation of the NHP and sidearm phosphorus atoms during the shipping/handling process (e.g. C₈₀H₆₇NiBN₂O₂P₄: C, 74.96; H, 5.27; N, 2.19).

[(PPOiPrP)Ni(PMe₃)(H)][BPh₄] (4). To a stirring solution of 3a (48 mg, 0.045 mmol) dissolved in THF (10 mL) was added isopropanol (6.8 µL, 0.089 mmol) via micropipette. The solution immediately turned yellow and was stirred at room temperature for 2 h. The solvent was removed from the reaction mixture in vacuo. The yellow solid was dissolved in C₆H₆ (5 mL) and filtered through Celite. The solvent was removed from the filtrate in vacuo, yielding 4 as a yellow solid (44 mg, 87%). Crystals of 4 suitable for X-ray diffraction were grown via vapor diffusion of *n*-pentane into a concentrated THF solution of 4 at -35 $^{\circ}$ C. ¹H NMR (600 MHz, CD₂Cl₂): δ 7.57-7.39 (m overlapping signals, Ar-H, 12H), 7.36-7.27 (m overlapping signals of BPh₄, 8H, and Ar-H, 2H), 7.24-7.09 (m overlapping signals, Ar-H, 14H), 7.02 (m, BPh₄, 8H), 6.87 (m, BPh₄, 4H), 4.32 (sept, O(CH)(CH₃)₂, ${}^{3}J_{H-H} = 6.3$ Hz, 1H), 3.96 (m, CH₂CH₂, 2H), 2.51 (m, CH₂CH₂, 2H), 1.14 (d, O(CH)(CH₃)₂, ${}^{3}J_{H-H} = 6.1 \text{ Hz}, 6\text{H}, 0.82 \text{ (d, P(CH₃)₃, }^{2}J_{H-PMe3} = 8.5 \text{ Hz}, 9\text{H}), -13.00$ (ddt, Ni-H, J = 21.0 Hz, J = 51.5 Hz, ${}^{2}J_{H-PNHP} = 221.3$ Hz, 1H). ${}^{31}P\{{}^{1}H\}$ NMR (242.9 MHz, CD₂Cl₂): δ 124.1 (m, P^{NHP}, 1P), 16.5 (dd, PPh₂, ²J_{P-} $PNHP = 76.3 \text{ Hz}, {}^{2}J_{P-PMe3} = 135.2 \text{ Hz}, 2P$, -18.9 (br t, PMe₃, ${}^{2}J_{P-PPh2} = 135.2 \text{ Hz}$) 135.8 Hz, 1P). ³¹P NMR (242.9 MHz, CD₂Cl₂): δ 124.1 (br dt, P^{NHP}, $^{2}J_{P-PPh2} = 76.8 \text{ Hz}, ^{2}J_{P-H} = 221.8 \text{ Hz}, 1P$), 16.5 (dd, PPh₂, $^{2}J_{P-PNHP} = 76.4$ Hz, ${}^{2}J_{P-PMe3}$ = 132.5 Hz, 2P), -18.9 (br t, PMe₃, ${}^{2}J_{P-PPh2}$ = 136.8 Hz, 1P). ¹³C{¹H} NMR (150.9 MHz, CD₂Cl₂): δ 164.5 (m, BPh₄-, ipso), 148.3 (m, ipso), 148.0 (m, ipso), 146.9 (m, ipso), 136.3 (s, BPh₄-), 135.5 (m, ispo), 135.0 (s), 133.7 (m), 133.2 (m), 133.0 (s), 130.9 (s), 130.8 (s),

129.3 (m), 128.9 (m), 126.0 (s, BPh₄), 124.3 (s), 123.5 (s), 122.1 (s, BPh₄), 72.1 (m, O(CH)(CH₃)₂), 49.4 (m, CH₂CH₂), 24.5 (m, O(CH)(CH₃)₂), 20.1 (m, P(CH₃)₃). 11 B NMR (192.5 MHz, CD₂Cl₂): δ -6.5. Repeated attempts to obtain satisfactory elemental analysis data for 4 were unsuccessful owing to its sensitivity to air and moisture and decomposition during the shipping/handling process. ESI-HRMS (C₄H₈O, positive mode): Calcd m/z for [(PP^{O/P}TP)Ni(PMe₃)]*: 803.2143. Found: 803.2141. ESI-HRMS (C₄H₈O, negative mode): Calcd m/z for [BPh₄]: 319.1657. Found: 319.1666.

(PP^{Ph}P)Ni(PMe₃) (5). Complex 3a (33 mg, 0.031 mmol) was suspended in dioxane (6 mL), heated to 80 °C, and allowed to stir for 1 h, resulting in a homogeneous solution. The solvent was removed from the resulting bright orange solution in vacuo. The remaining orange solid was washed with hexanes (6 mL), extracted with C₆H₆ (4 mL), and filtered through Celite. The solvent was removed from the filtrate in vacuo, yielding 5 as an orange solid (24 mg, 95%). Crystals of 5 suitable for X-ray diffraction were grown via layering a concentrated C₆H₆ solution of **5** with *n*-pentane. ¹H NMR (600 MHz, C₆D₆): δ 7.75 (m, Ar-H, 4H), 7.56 (m, Ar-H, 4H), 7.38 (m, P^{NHP}-C₆H₅, 2H), 7.32 (m, Ar-H, 2H), 7.25-7.21 (m, PNHP-C₆H₅, 1H), 7.10 (m, Ar-H, 4H), 7.04-7.00 (m, Ar-H, 4H), 6.99-6.94 (m, P^{NHP} -C₆H₅, 2H), 6.89-6.85 (m overlapping signals, Ar-H, 6H), 6.74-6.69 (m overlapping signals, Ar-H, 4H), 3.21 (m, CH₂CH₂, 2H), 2.69 (m, CH₂CH₂, 2H), 0.82 (d, P(CH₃)₃, ${}^{2}J_{H-P} = 5.1 \text{ Hz}, 9\text{H}$). ${}^{31}P\{{}^{1}H\}$ NMR (242.9 MHz, C₆D₆): δ 89.3 (d, P^{NHP} , ${}^{2}J_{P-PMe3} = 29.3 \text{ Hz}, 1P$), 23.3 (d, PPh₂, ${}^{2}J_{P-PMe3} = 20.5 \text{ Hz}, 2P$), -20.7 (dt, PMe₃, ${}^{2}J_{P-PPh2} = 19.8 \text{ Hz}$, ${}^{2}J_{P-PNHP} = 29.3 \text{ Hz}$, 1P). ${}^{13}C\{{}^{1}H\}$ NMR (150.9) MHz, C₆D₆): δ 151.1 (m, *ipso*), 148.6 (m, *ipso*), 141.9 (m, *ipso*), 135.7 (m, ipso), 134.4 (s), 133.7 (m), 130.0 (s), 128.6 (s), 128.4 (m), 128.3 (s), 128.1 (m, overlapping with C₆D₆), 128.0 (m, overlapping with C₆D₆), 127.7 (s), 127.6 (s), 127.4 (m), 126.6 (m, ipso), 119.7 (s), 118.4 (s), 46.3 (s, CH₂CH₂), 21.3 (m, P(CH₃)₃). Owing to the reactivity of 5 with air and moisture, repeated attempts for satisfactory elemental analysis and/or high-resolution ESI-MS data could not be obtained.

(PPHP)Ni(PMe₃) (6). Complex 2a (397 mg, 0.509 mmol) was dissolved by stirring in THF (100 mL). A suspension of LiAlH₄ (19.3 mg, 0.509 mmol) in THF (25 mL) was added to the stirring solution of 2a. The solution immediately turned a deeper orange color and was stirred at room temperature for 2 h. The solution was then filtered through Celite, and the solvent was removed from the filtrate in vacuo. The remaining solid was extracted with C₆H₆ (100 mL) and filtered through Celite once more. The solvent was removed from the filtrate in vacuo, yielding 6 as an orange solid (313 mg, 83%). Crystals of 6 suitable for X-ray diffraction were grown via layering a concentrated C₆H₆ solution of 6 with *n*-pentane. ¹H NMR (400 MHz, C_6D_6): δ 7.78 (m, Ar-H, 4H), 7.56 (m, Ar-H, 4H), 7.31 (dt, P^{NHP} -H, ${}^{1}J_{H-PNHP} = 246.9$ Hz, ${}^{2}J_{H-PPh2} =$ 12.9 Hz, 1H), 7.29 (m, Ar-H, 2H), 7.14-7.10 (m overlapping signals, Ar-H, 6H), 7.05 (m, Ar-H, 2H), 6.88-6.83 (m overlapping signals, Ar-H, 6H), 6.69 (m, Ar-H, 2H), 6.64 (m, Ar-H, 2H), 3.26 (m, CH₂CH₂, 2H), 2.87 (m, CH₂CH₂, 2H), 0.93 (d, P(CH₃)₃, ${}^{2}J_{H-PPMe3} = 5.2$ Hz, 9H). $^{31}P\{^{1}H\}$ NMR (242.9 MHz, C₆D₆): δ 75.3 (d, P^{NHP} , $^{2}J_{P-PMe3} = 26.4$ Hz, 1P), 25.5 (d, PPh₂, ${}^{2}J_{P-PMe3}$ = 17.6 Hz, 2P), -19.3 (dt, PMe₃, ${}^{2}J_{P-PNHP}$ = 24.6 Hz, ${}^{2}J_{P-PMe3} = 17.6$ Hz, 1P). ${}^{31}P$ NMR (242.9 MHz, C₆D₆): δ 75.3 (dd, P^{NHP} , ${}^{I}J_{P-H} = 247.1 \text{ Hz}$, ${}^{2}J_{P-PMe3} = 26.2 \text{ Hz}$, 1P), 25.5 (br s, PPh₂, 2P), -19.3 (m, PMe₃, 1P). ¹³C{¹H} NMR (150.9 MHz, C₆D₆): δ 149.7 (m, ipso), 142.0 (m, ipso), 141.4 (m, ipso), 134.0 (s), 133.8 (m), 129.7 (s), 128.6 (s), 128.4 (s), 128.0 (m, overlapping with C₆D₆), 127.9 (m, overlapping with C₆D₆), 127.5 (m), 126.1 (m, *ipso*), 119.7 (s), 118.1 (s), 48.2 (d, CH₂CH₂, ${}^{2}J_{C-PNHP} = 7.4$ Hz), 21.8 (m, P(CH₃)₃). IR (C₆H₆): 2072 cm⁻¹. IR (ATR): 2064 cm⁻¹. Owing to the reactivity of 6 with air and moisture, repeated attempts for satisfactory elemental analysis and/or high-resolution ESI-MS data could not be obtained.

(PP^DP)Ni(PMe₃) (6-d). 6-d was synthesized via an analogous procedure for 6 using LiAlD₄. Complex 2a (34.9 mg, 44.8 μmol) was dissolved by stirring in THF (6 mL). A suspension of LiAlD₄ (1.9 mg, 0.045 mmol) in THF (4 mL) was added to the stirring solution of 2a. The solution immediately turned a deeper orange color and was stirred at room temperature for 2 h. The solution was then filtered through Celite, and the solvent was removed from the filtrate *in vacuo*. The remaining solid was extracted with C₆H₆ (5 mL) and filtered through Celite once more. The solvent was removed from the filtrate *in vacuo*, yielding 6-d as an orange solid (30.9 mg, 92%). ¹H and ³¹P{¹H} NMR

data of **6-d** were nearly identical to **6** except for the absence of the P^{NHP}-H peak at 7.31 ppm in the ¹H NMR spectrum. ¹H NMR (600 MHz, C₆D₆): δ 7.77 (m, Ar-H, 4H), 7.55 (m, Ar-H, 4H), 7.28 (m, Ar-H, 2H), 7.14-7.10 (m overlapping signals, Ar-H, 6H), 7.04 (m, Ar-H, 2H), 6.89-6.83 (m overlapping signals, Ar-H, 6H), 6.68 (m, Ar-H, 2H), 6.64-6.61 (m, Ar-H, 2H), 3.24 (m, CH₂CH₂, 2H), 2.86 (m, CH₂CH₂, 2H), 0.92 (d, P(CH₃)₃, ²J_{H-PMe3} = 5.2 Hz, 9H). ²H NMR (92.1 MHz, C₆H₆): δ 7.31 (d, P^{NHP}-D, ¹J_{D-PNHP} = 38.8 Hz, 1D). ³¹P {¹H} NMR (242.9 MHz, C₆D₆): δ 73.5 (dt, P^{NHP}, ²J_{P-Phh2} = 38.4 Hz, ²J_{P-PMe3} = 26.5 Hz, 1P), 24.9 (d, PPh₂, ²J_{P-PMe3} = 17.6 Hz, 2P), -19.9 (dt, PMe₃, ²J_{P-PNHP} = 26.7 Hz, ²J_{P-PPh2} = 17.0 Hz, 1P). ³¹P NMR (242.9 MHz, C₆D₆): δ 73.5 (m, P^{NHP}, 1P), 24.9 (br s, PPh₂, 2P), -19.9 (m, PMe₃, 1P).

[PPP]H (8). KBEt₃H (2.32 mL, 1.0 M solution in THF, 2.32 mmol) was added via a glass syringe to a stirring solution of 1 (1.50 g, 2.33 mmol) dissolved in THF (250 mL). The solution immediately turned yellow and was stirred at room temperature for 2 h. The solution was then filtered through Celite, and the solvent was removed from the filtrate in vacuo. The remaining solid was washed with hexanes (80 mL) and C₆H₆ (20 mL), removing a yellow filtrate. The remaining white solid was extracted with additional C₆H₆ (100 mL) and filtered through Celite once more. The solvent was removed from the filtrate in vacuo, yielding **8** as a white solid (1.10 g, 78%). 1 H NMR (400 MHz, C₆D₆): δ 7.46-7.42 (m, Ar-H, 4H), 7.39-7.34 (m, Ar-H, 4H), 7.31-7.27 (m, Ar-H H, 2H), 7.09-6.98 (m overlapping signals, Ar-H, 14H), 6.88 (dt, PNHP-H, J = 3.7 Hz, ${}^{1}J_{H-P} = 235.0$ Hz, 1H), 6.78-6.74 (m, Ar-H, 2H), 6.73 (bt, Ar-H, J = 7.6 Hz, 2H), 3.45 (m, CH₂CH₂, 2H), 3.04 (m, CH₂CH₂, 2H). ³¹P{¹H} NMR (242.9 MHz, C₆D₆): δ 51.6 (t, P^{NHP}, $J_{P-PPh2} = 206.1$ Hz, 1P), -18.1 (d, PPh₂, $J_{P-PNHP} = 205.8$ Hz, 2P). ³¹P NMR (162.0 MHz, C_6D_6): δ 51.6 (dt, P^{NHP} , $J_{P-PPh2} = 206.5$ Hz, ${}^{1}J_{P-H} = 235.9$ Hz, 1P), -18.1 (d, PPh₂, J_{P-PNHP} = 207.1 Hz, 2P). ¹³C{¹H} NMR (150.9 MHz, C₆D₆): δ 153.3 (m), 139.0 (m), 138.5 (m), 136.7 (s), 133.8 (m), 130.6 (s), 128.6 (m), 128.5 (s), 128.2 (s), 127.7 (m), 121.6 (s), 117.5 (s), 51.9 (d, CH_2CH_2 , J = 6.6 Hz). IR (C_6H_6): 2245 cm⁻¹; 2125 cm⁻¹. Anal. Calcd for C₃₈H₃₃N₂P₂: C, 74.75; H, 5.45; N, 4.59. Found: C, 71.17; H, 5.24; N, 4.28. Compound 8 is extremely air and moisture sensitive. Repeated attempts to acquire satisfactory microanalysis data resulted in data that was consistent with partial phosphine oxidation during sample handling and can explain the low C value (e.g. $C_{38}H_{33}N_2P_3 + 2O$: C, 71.03; H, 5.18; N, 4.26). ESI-HRMS (C₄H₈O, positive mode): Calcd m/z for [(PPP)]+: 609.1773. Found: 609.1788.

(PPHP)Pd(PPh₃) (9). To a stirring solution of 8 (93.5 mg, 0.153 mmol) dissolved in THF (4 mL) was added a solution of Pd(PPh₃)₄ (177 mg, 0.153 mmol) dissolved in THF (6 mL). The solution gradually turned a deep orange-green color and was stirred at room temperature for 2 h. THF was then removed from the reaction mixture in vacuo. The dark orange-green solid was extracted with hexanes (18 mL) into a 20mL vial as a lime-green solution and placed in a freezer at -35 °C overnight. Green precipitate formed in the vial, and hexanes was decanted via pipet. The remaining green solid was extracted with C₆H₆ (5 mL), and the solvent was removed in vacuo to yield 9 as a green solid (139 mg, 93%). ¹H NMR (600 MHz, C₆D₆): δ 7.53-7.50 (m, Ar-H, 4H), 7.49-7.46 (m, Ar-H, 6H), 7.27-7.22 (m overlapping signals, Ar-H, 6H), 7.09 (m, Ar-H, 3H), 6.98-6.95 (m, Ar-H, 2H), 6.94-6.90 (m, Ar-H, 6H), 6.89-6.86 (m, Ar-H, 4H), 6.80-6.78 (m overlapping signals, Ar-H, 8H), 6.74-6.69 (m overlapping signals, Ar-H, 4H), 3.24 (m, CH₂CH₂, 2H), 2.75 (m, CH₂CH₂, 2H). The P^{NHP}-H proton could not be located and assigned due to overlapping aromatic signals. $^{31}P\{^{1}H\}\ NMR\ (242.9$ MHz, C₆D₆): δ 78.0 (dt, P^{NHP}, ${}^{2}J_{P-PPh2} = 15.1$ Hz, ${}^{2}J_{P-PPh3} = 26.2$ Hz, 1P), 32.6 (dt, PPh₃, ${}^{2}J_{P-PPh_2} = 20.4$ Hz, ${}^{2}J_{P-PNHP} = 26.5$ Hz, 1P), 9.4 (dd, PPh₂, ${}^{2}J_{P-PNHP}$ = 15.0 Hz, ${}^{2}J_{P-PPh_3}$ = 19.9 Hz, 2P). ${}^{31}P$ NMR (242.9 MHz, C₆D₆): δ 78.0 (bd, NHP , ${}^{1}J_{P-H}$ = 205.9 Hz, 1P), 32.6 (bs, PPh₃, 1P), 9.4 (bs, PPh₂, 2P). ${}^{13}C\{{}^{1}H\}$ NMR (150.9 MHz, C₆D₆): δ 149.3 (m, *ipso*), 141.3 (m, ipso), 140.9 (m, ipso), 140.4 (m, ipso), 134.6 (s), 134.4 (m), 134.1 (m), 133.7 (m), 129.9 (s), 129.3 (m, *ipso*), 128.8 (m), 128.6 (s), 128.3 (s), 128.0 (m, overlapping with C_6D_6), 127.8 (m), 127.7 (s), 120.9(s), 120.8 (s), 49.6 (d, CH₂CH₂, ${}^{2}J_{C-PNHP}$ = 8.8 Hz). IR (C₆H₆): 2061 cm⁻¹ 1. Owing to the reactivity of **9** with air and moisture, repeated attempts for satisfactory elemental analysis and/or high-resolution ESI-MS data could not be obtained.

X-ray Crystallography Procedures. Single crystal X-ray diffraction studies were carried out on a Bruker D8 Venture Kappa Photon II or III CPAD diffractometer equipped with Mo K_{α} radiation (λ = 0.71073 Å). Data were collected in a nitrogen gas stream at 100(2) K (Oxford Cryosystems Cryostream 700) using φ and ω scans. The data were integrated using the Bruker SAINT software program and scaled using the SADABS software program within the APEX4 GUI.³⁷ Solution by dual-space method (SHELXT v2018/2) produced a complete phasing model for refinement.³⁸ Refinement was performed within the OLEX2³⁹ GUI using SHELXL⁴⁰ (v2019/1). All nonhydrogen atoms were refined anisotropically by full-matrix least-squares (SHELXL).⁴⁰ All carbon-bonded hydrogen atoms were placed using a riding model. Their positions were constrained relative to their parent atom using the appropriate HFIX command in SHELXL. All other hydrogen atoms (Ni- and P-bonding) were located in the difference map. Their relative positions and thermal parameters were freely refined. Publication figures were generated with Mercury. 41 Crystallographic details are summarized in Tables S1-S2 of the Supporting Information.

Computational Details. All calculations were performed using Gaussian16 for the Linux operating system.⁴² DFT calculations were carried out using the M06 functional.⁴³ A mixed basis set was employed, using the LANL2DZ(p,d) double- ζ basis set with effective core potentials for P and Ni atoms^{44–47} and Gaussian 16's internal LANL2DZ basis (equivalent to D95V) for C, H, N, and O atoms. 48 This basis set and functional combination was chosen based on a previous investigation of 8 different functional and basis set combinations using related (PPP)Co systems and choosing the combination that attained an optimized geometry closest to the X-ray derived experimental geometry (M-P distances) while minimizing computational resources.⁴⁹ Starting from crystallographically determined coordinates, the geometries of 3a, 3b, and 4 were optimized to a minimum and counterions were omitted for simplicity. Subsequent frequency calculations were carried out to confirm the absence of imaginary frequencies. NBO⁵⁰ calculations were then performed on the optimized geometries of 3a, 3b, and 4. Deletion energies (E^{del}) represent the change in energy upon zeroing the matrix elements corresponding to the 3d(Ni)→p(P) donor-acceptor interactions.⁵¹ XYZ coordinates of the optimized geometries of **3a**, **3b**, and 4 are provided in Tables S3, S4, and S7 of the Supporting Infor-

ASSOCIATED CONTENT

Supporting Information

The Supporting Information is available free of charge on the ACS Publications website.

Crystallographic data, DFT calculation results, XYZ coordinates for optimized structures, spectroscopic data for **2-9** (PDF).

Accession Codes

CCDC 2196224-2196229 contain the supplementary crystallographic data for this paper. These data can be obtained free of charge via www.ccdc.cam.ac.uk/data_request/cif, or by emailing data_request@ccdc.cam.ac.uk, or by contacting The Cambridge Crystallographic Data Centre, 12 Union Road, Cambridge CB2 1EZ, UK; fax: +44 1223 336033.

AUTHOR INFORMATION

Corresponding Author

Christine M. Thomas – Department of Chemistry and Biochemistry, The Ohio State University, Columbus, Ohio 43210, United States; orcid.org/0000-0001-5009-0479; Email: thomasc@chemistry.ohio-state.edu*

Notes

The authors declare no competing financial interest.

ACKNOWLEDGMENT

This material is based upon work supported by the National Science Foundation under Grant CHE-2101002. The Ohio State University Department of Chemistry and Biochemistry and The Ohio State University Sustainability Institute are gratefully acknowledged for financial support. The authors thank Dr. Alicia Friedman for their generous help in collecting high-resolution ESI-MS data.

REFERENCES

- (1) Hopkinson, M. N.; Richter, C.; Schedler, M.; Glorius, F. An Overview of N-Heterocyclic Carbenes. *Nature* **2014**, *510*, 485– 496.
- (2) Bourissou, D.; Guerret, O.; Gabbaı, F. P.; Bertrand, G. Stable Carbenes. Chem. Rev. 2000, 100, 39–91.
- (3) Gudat, D.; Haghverdi, A.; Hupfer, H.; Nieger, M. Stability and Electrophilicity of Phosphorus Analogues of Arduengo Carbenes-An Experimental and Computational Study. *Chem. Eur. J.* **2000**, *6*, 3414–3425.
- (4) Gudat, D. Cation Stabilities, Electrophilicities, and "Carbene Analogue" Character of Low Coordinate Phosphorus Cations. Eur. J. Inorg. Chem. 1998, 1087–1094.
- (5) Gudat, D. Cationic Low Coordinated Phosphorus Compounds as Ligands: Recent Developments. Coord. Chem. Rev. 1997, 163, 71–106
- (6) Rosenberg, L. Metal Complexes of Planar PR₂ Ligands: Examining the Carbene Analogy. Coord. Chem. Rev. 2012, 256, 606–626.
- (7) Nakazawa, H. Transition Metal Complexes Bearing a Phosphenium Ligand. *Adv. Organomet. Chem.* **2004**, *50*, 107–143.
- (8) Birchall, N.; Feil, C. M.; Gediga, M.; Nieger, M.; Gudat, D. Reversible Cooperative Dihydrogen Binding and Transfer with a Bis-Phosphenium Complex of Chromium. *Chem. Sci.* 2020, 11, 9571–9576.
- (9) Gediga, M.; Feil, C. M.; Schlindwein, S. H.; Bender, J.; Nieger, M.; Gudat, D. N-Heterocyclic Phosphenium Complex of Manganese: Synthesis and Catalytic Activity in Ammonia Borane Dehydrogenation. *Chem. Eur. J.* 2017, 23 (48), 11560–11569.
- (10) Poitras, A. M.; Bezpalko, M. W.; Foxman, B. M.; Thomas, C. M. Cooperative Activation of O-H and S-H Bonds across the Co-P Bond of an N-Heterocyclic Phosphido Complex. *Dalton Trans*. 2019, 48 (9), 3074–3079.
- (11) Poitras, A. M.; Knight, S. E.; Bezpalko, M. W.; Foxman, B. M.; Thomas, C. M. Addition of H₂ Across a Cobalt–Phosphorus Bond. *Angew. Chem. Int. Ed.* **2018**, *57* (6), 1497–1500.
- (12) Pan, B.; Bezpalko, M. W.; Foxman, B. M.; Thomas, C. M. Heterolytic Addition of E-H Bonds across Pt-P Bonds in Pt N-Heterocyclic Phosphenium/Phosphido Complexes. *Dalton Trans.* **2012**, *41* (30), 9083–9090.
- (13) Hutchins, L. D.; Paine, R. T.; Campana, C. F. Structure and Bonding in a Phosphenium Ion-Metal Complex, CH₃NCH₂CH₂N(CH₃)PMo(η⁵-C₅H₅)(CO)₂. An Example of a Molybdenum-Phosphorus Multiple Bond. J. Am. Chem. Soc. 1980, 102, 4521–4523.
- (14) Burck, S.; Daniels, J.; Gans-Eichler, T.; Gudat, D.; Nattinen, K.; Nieger, M. N-Heterocyclic Phosphenium, Arsenium, and Stibenium Ions as Ligands in Transition Metal Complexes: A Comparative Experimental and Computational Study. Z. Anorg. Allg. Chem. 2005, 631, 1403.
- (15) Hutchins, L. D.; Duesler, E. N.; Paine, R. T. Structure and Bonding in a Phosphenium Ion-Iron Complex, Fe[η⁵-(CH₃)₅C₅](CO)₂[PN(CH₃)CH₂CH₂NCH₃]. A Demonstration of Phosphenium Ion Acceptor Properties. *Organometallics* **1982**, *1*, 1254–1256.
- (16) Pan, B.; Xu, Z.; Bezpalko, M. W.; Foxman, B. M.; Thomas, C. M. N-Heterocyclic Phosphenium Ligands as Sterically and Electronically-Tunable Isolobal Analogues of Nitrosyls. *Inorg. Chem.* 2012, 51 (7), 4170–4179.
- (17) Pan, B.; Bezpalko, M. W.; Foxman, B. M.; Thomas, C. M. Coordination of an N-Heterocyclic Phosphenium Containing Pincer Ligand to a Co(CO)₂ Fragment Allows Oxidation to Form an Unusual N-Heterocyclic Phosphinito Species.

 Organometallics 2011, 30 (21), 5560–5563.
- (18) Caputo, C. A.; Jennings, M. C.; Tuononen, H. M.; Jones, N. D.

- Phospha-Fischer Carbenes: Synthesis, Structure, Bonding, and Reactions of Pd(0)- and Pt(0)-Phosphenium Complexes. *Organometallics* **2009**, *28*, 990–1000.
- (19) Roncaroli, F.; Videla, M.; Slep, L. D.; Olabe, J. A. New Features in the Redox Coordination Chemistry of Metal Nitrosyls {M-NO⁺; M-NO⁺; M-NO⁻(HNO)}. Coord. Chem. Rev. 2007, 251, 1903–1930.
- (20) Day, G. S.; Pan, B.; Kellenberger, D. L.; Foxman, B. M.; Thomas, C. M. Guilty as Charged: Non-Innocent Behavior by a Pincer Ligand Featuring a Central Cationic Phosphenium Donor. *Chem. Commun.* 2011, 47 (12), 3634–3636.
- (21) Evers-McGregor, D. A.; Bezpalko, M. W.; Foxman, B. M.; Thomas, C. M. N-Heterocyclic Phosphenium and Phosphido Nickel Complexes Supported by a Pincer Ligand Framework. *Dalton Trans.* 2016, 45 (5), 1918–1929.
- (22) Cowley, A. H.; Kemp, R. A. Synthesis and Reaction Chemistry of Stable Two-Coordinate Phosphorus Cations (Phosphenium Ions). *Chem. Rev.* **1985**, *85* (5), 367–382.
- Yang, L.; Powell, D. R.; Houser, R. P. Structural Variation in Copper(I) Complexes with Pyridylmethylamide Ligands: Structural Analysis with a New Four-Coordinate Geometry Index, τ₄. Dalton Trans. 2007, 955–964.
- (24) Bezpalko, M. W.; Foxman, B. M.; Thomas, C. M. Use of a Bidentate Ligand Featuring an N-Heterocyclic Phosphenium Cation (NHP⁺) to Systematically Explore the Bonding of NHP⁺ Ligands with Nickel. *Inorg. Chem.* **2015**, *54* (17), 8717–8726.
- (25) Stadelmann, B.; Bender, J.; Förster, D.; Frey, W.; Nieger, M.; Gudat, D. An Anionic Phosphenium Complex as an Ambident Nucleophile. *Dalton Trans.* 2015, 44 (13), 6023–6031.
- (26) Pauling, L. *The Nature of the Chemical Bond*; Cornell Univ. Press: Ithaca, New York, 1960.
- (27) Addison, A. W.; Rao, T. N.; Reedijk, J.; van Rijn, J.; Verschoor, G. C. Synthesis, Structure, and Spectroscopic Properties of Copper(II) Compounds Containing Nitrogen-Sulphur Donor Ligands; the Crystal and Molecular Structure of Aqua[1,7-bis(N-methylbenzimidazol-2'-yl)-2,6-dithiaheptane]copper(II) Perchlorate. J. Chem. Soc. Dalton Trans. 1984, 1349–1356.
- (28) Knight, S. E.; Bezpalko, M. W.; Foxman, B. M.; Thomas, C. M. Coordination of N-Heterocyclic Phosphine- and Phosphenium-Containing Pincer Ligands to Copper(I): Evidence for Reactive Electrophilic Metal-Phosphenium Intermediates. *Inorganica Chim. Acta* 2014, 422, 181–187.
- (29) Aresta, M.; Quaranta, E.; Tommasi, I. Tetraphenylborate Anion as a Phenylating Agent: Chemical and Electrochemical Reactivity of BPh₄-Rh Complexes toward Mono- and Dienes and Carbon Dioxide. *Organometallics* **1995**, *14* (11), 3349–3356.
- (30) Snow, S. S.; Jiang, D.-X.; Parry, R. W. Preparation of New Bis(dialkylamino) Phosphine Species via Redcution of Bis(dialkylamino)halophosphines. *Inorg. Chem.* **1985**, *24*, 1460–1463.
- (31) Heurich, T.; Qu, Z.; Kunzmann, R.; Schnakenburg, G.; Engeser, M.; Nozinovic, S.; Streubel, R. Styrene Polymerization under Ambient Conditions by Using a Transient 1,3,2-Diazaphospholane-2-oxyl Complex. Chem. Eur. J. 2018, 24, 6473–6478.
- (32) Feil, C. M.; Hettich, T. D.; Beyer, K.; Sondermann, C.; Schlindwein, S. H.; Nieger, M.; Gudat, D. Comparing the Ligand Behavior of N-Heterocyclic Phosphenium and Nitrosyl Units in Iron and Chromium Complexes. *Inorg. Chem.* 2019, 58, 6517–6528.
- (33) Hatzis, G. P.; Oliemuller, L. K.; Dickie, D. A.; Thomas, C. M. N-Heterocyclic Phosphido Complexes of Rhodium Supported by a Rigid Pincer Ligand. Eur. J. Inorg. Chem. 2020, 2873–2881.
- (34) Welch, G. C.; Stephan, D. W. Facile Heterolytic Cleavage of Dihydrogen by Phosphines and Boranes. J. Am. Chem. Soc. 2007, 129, 1880-1881.
- (35) Blackwell, J. M.; Sonmor, E. R.; Scoccitti, T.; Piers, W. E. B(C₆F₅)₃-Catalyzed Hydrosilation of Imines via Silyliminium Intermediates. *Org. Lett.* **2000**, *2* (24), 3921-3923.
- (36) Fulmer, G. R.; Miller, A. J. M.; Sherden, N. H.; Gottlieb, H. E.; Nudelman, A.; Stoltz, B. M.; Bercaw, J. E.; Goldberg, K. I. NMR Chemical Shifts of Trace Impurities: Common Laboratory Solvents, Organics, and Gases in Deuterated Solvents Relevant to the Organometallic Chemist. *Organometallics* 2010, 29 (29), 2176–2179.

- (37) Apex4; SAINT, v. 8.40b; SADABS, v. 2016/2. Bruker AXS, Inc.:Madison, Wisconsin, USA, 2016.
- (38) Sheldrick, G. M. SHELXT Integrated Space-Group and Crystal-Structure Determination. *Acta Crystallogr, Sect. A: Found. Adv.* **2015**. *71*, 3–8.
- (39) Dolomanov, O. V; Bourhis, L. J.; Gildea, R. J.; Howard, J. A. K.; Puschmann, H. OLEX2: A Complete Structure Solution, Refinement, and Analysis Program. J. Appl. Crystallogr. 2009, 42 (2), 339–341.
- (40) Sheldrick, G. M. Crystal Structure Refinement with SHELXL. *Acta Crystallogr., Sect. C: Struct. Chem.* **2015**, 71 (1), 3–8.
- (41) Macrae, C. F.; Bruno, I. J.; Chisholm, J. A.; Edgington, P. R.; McCade, P.; Pidcock, E.; Rodriquez-Monge, L.; Taylor, R.; Van de Streek, J.; Wood, P. A. Merucry CSD 2.0 - New Features for the Visualization and Investigation of Crystal Structures. J. Appl. Crystallogr. 2008, 41 (2), 466–470.
- Frisch, M. J.; Trucks, G. W.; Schlegel, H. B.; Scuseria, G. E.; (42)Robb, M. A.; Cheeseman, J. R.; Scalmani, G.; Barone, V.; Petersson, G. A.: Nakatsuii, H.: Li, X.: Caricato, M.: Marenich. A. V.; Bloino, J.; Janesko, B. G.; Gomperts, R.; Mennucci, B.; Hratchian, H. P.; Ortiz, J. V.; Izmaylov, A. F.; Sonnenberg, J. L.; Williams Ding, F.; Lipparini F.; Egidi, F.; Goings, J.; Peng, B.; Petrone, A.; Henderson, T.; Ranasinghe, D.; Zakrzewski, V. G.; Gao, J.; Rega, N.; Zheng, G.; Liand, W.; Hada, M.; Ehara, M.; Toyota, K.; Fukuda, R.; Hasegawa, J.; Ishida, M.; Nakajima, T.; Honda, Y.; Kitao, O.; Nakai, H.; Vreven, T.; Throssell, K.; Montgomery, J. A., Jr.; Peralta, J. E.; Ogliaro, F.; Bearpark, M. J.; Hyed, J. J.; Brothers, E. N.; Kudin, K. N.; Staroverov, V. N.; Keith, T. A.; Kobayashi, R.; Normand, J.; Raghavachari, K.; Rendell, A. P.; Burant, J. C.; Iyengar, S. S.; Tomasi, J.; Cossi, M.; Millam, J. M.; Klene, M.; Adamo, C.; Cammi, R.; Ochterski, J. W.; Martin, R. L.; Morokuma, K.; Farkas, O.; Foresman, J. B.;

- Fox, D. J. Gaussian 16, rev. C.01; Gaussian, Inc.: Wallingford, CT. 2016.
- (43) Zhao, Y.; Truhlar, D. G. The M06 Suite of Density Functionals for Main Group Thermochemistry, Thermochemical Kinetics, Noncovalent Interactions, Excited States, and Transition Elements: Two New Functionals and Systematic Testing of Four M06-Class Functionals and 12 Other Functionals. *Theor. Chem.* Acc. 2008, 120, 215–241.
- (44) Hay, P. J.; Wadt, W. R. Ab Initio Effective Core Potentials for Molecular Calculations. Potentials for K to Au Including the Outermost Core Orbitals. J. Chem. Phys. 1985, 82, 299–310.
- (45) Hay, P. J.; Wadt, W. R. Ab Initio Effective Core Potentials for Molecular Calculations. Potentials for the Transition-Metal Atoms Sc to Hg. J. Chem. Phys. 1985, 82, 270–283.
- (46) Wadt, W. R.; Hay, P. J. Ab Initio Effective Core Potentials for Molecular Calculations. Potentials for Main Group Elements Na to Bi. J. Chem. Phys. 1985, 82, 284–298.
- (47) Roy, L. E.; Hay, P. J.; Martin, R. L. Revised Basis Sets for the LANL Effective Core Potentials. J. Chem. Theory Comput. 2008, 4, 1029–1031.
- (48) Dunning, T. H.; Hay, P. J. In *Modern Theoretical Chemistry*; Schaefer, H. F., Ed.; Plenum: New York, 1976; Vol. 3, pp 1-28.
- (49) Poitras, A. M.; Bezpalko, M. W.; Moore, C. E.; Dickie, D. A.; Foxman, B. M.; Thomas, C. M. A Series of Dimeric Cobalt Complexes Bridged by N-Heterocylic Phosphido Ligands. *Inorg. Chem.* 2020, 59, 4729-4740.
- (50) Glendening, E. D.; Reed, A. E.; Carpenter, J. E.; Weinhold, F. *NBO*, Version 3.1.
- (51) Reed, A. E.; Curtiss, L. A.; Weinhold, F. Intermolecular Interactions from a Natural Bond Orbital, Donor-Acceptor Viewpoint. Chem. Rev. 1988, 88, 899–926.

TOC Graphic and Synopsis

N-heterocyclic phosphenium complexes of nickel are reported and compared to their group 10 analogues, revealing subtle differences in structure and bonding. Structural comparisons, computational methods, and reactivity studies are used to compare the dominant resonance forms in the Ni/Pd/Pt series.

